Synthesis of ZSM-5 zeolite of improved bulk and surface properties via mixed templates

Mohamed Mokhtar Mohamed · F. I. Zidan · M. H. Fodail

Abstract Hydrothermally synthesized ZSM-5 zeolites using tetrapropyl-ammonium bromide (TPA-Br), Xylitol (Xy) and tetrapropyl-ammonium bromide + Xylitol templates; those compared with that of the parent having the same Si/Al molar ratio (64) and purchased from Mobil, were characterized with several physicochemical techniques including N_2 adsorption, XRD, TG/DSC, FTIR and pyridine-FTIR. The effect of various templates on the crystallinity, crystallites size, surface properties and thermal stabilities of the produced ZSM-5 were investigated. ZSM-5 synthesized using TPA-Br + Xy; of $S_{BET} = 393$ m^2 g^{-1}, exhibited a crystallinity percentage comprises of 142% when compared with that of the parent (taken at 100% crystallinity) and measured as well a crystallites size of 61 nm exceeding that derived from Xy (41 nm) that measured the lowest crystallinity percentages (71%), lowest S_{BET} (303 m^2 g^{-1}) and highest yield (65%) between all samples. The former sample showed high thermal stability (till 1,000 °C) when compared with that derived from TPA-Br, as illustrated from TG/DSC thermograms that provided a criteria on decreasing the pore radius as a result of enclosing appreciable amounts of TPA$^+$ and Xy inside narrow pores of ZSM-5. This sample also indicated a hydrophobic tendency when compared with that devoted from TPA-Br. Pyridine adsorption measurements showed that addition of Xy to TPA-Br stimulate the existence of basic sites in addition to acidic ones (mainly Brönsted ones) that was in the middle between that derived from Xy and TPA-Br templates. More infomations on the textural properties, morphologies, vibrational tetrahedral co-ordination T(Si or Al)–O modes and acidity were evaluated and discussed.

Introduction

ZSM-5 zeolite of a medium-pore with ellipsoidal tubular pores and maximum aperture of 0.56 nm has received much attention because of its optimum performances as solid acid catalyst in various industrial processes [1, 2]. It is well known that the internal surface of ZSM-5 micropores affects both the activity and selectivity rather than external ones when it is used as a catalyst [3]. Indeed, the micropore-structure of ZSM-5 hinders bulkier molecules greater than 0.56 nm to intervene the internal surfaces and thus inhibit and/ or limit the accessibility of internal active sites to the reactant molecules.

Nanostructured materials specifically zeolites, on the other hand, have received much attention in the last decade due to their unique physical, chemical and electronic properties [4]. Nanostructured zeolites that are still in its primary stages were found capable of decomposing many organic pollutants especially when supported a photocatalyst such as TiO_2 or Fe_2O_3 oxides [5, 6]. This is because of the advantages ZSM-5

M. M. Mohamed (✉)
Chemistry Department, Faculty of Science, Benha
University, Benha, Egypt
e-mail: mohmok2000@yahoo.com

F. I. Zidan · M. H. Fodail
Chemistry Department, Faculty of Science, Al-Azhar
University, Nasr City, Cairo, Egypt

have such as high surface area, decreasing particles size (if possible) and its heterogeneous nature; specifically, in liquid phase reactions and the facile retaining back the catalyst without lose. Upon decreasing the crystal size, the diffusional paths of the reactant and product molecules inside the pores become shorter, and this can result in a reduction or elimination of undesired diffusional limitations of the reaction rate.

One of the parameters that affect the textural properties of synthesized zeolite is the templating agent. That has a profound influence in structuring zeolite channels and controls the selectivity towards specific products during applying a reaction. Recently, a new family of microporous molecular sieves has been synthesized in a wide range of temperatures and pH via dissociating supramolecular templates into many single surfactant molecules [7, 8]. It has been found that the formation of ZSM-5 (Si:Al = ∞) was favored under the conditions of temperatures higher than 150 °C and surfactants with shorter alkyl chain lengths like $n \sim 6$ and 8. When increasing the temperature to 200 °C, mixtures of ZSM-5, ZSM-48 and dense phases were obtained by using the surfactants with longer alkyl chain lengths ($n \sim 8 \pm 14$) [9].

From the aspect of colloid chemistry, using a mixed surfactant template is an easy way to change the surface charge distribution and the packing parameters of the surfactant aggregates, and hence provides a favorable route to synthesis of porous materials with different pore sizes and structures. Therefore, mixed surfactant systems with unique aggregation behavior share many superiorities over single surfactant systems [10–16].

Therefore, it would be interesting to enter into further study on the synthesis of microporous molecular sieve using surfactants because it would give us a full understanding of the role of the surfactants in both synthesizing microporous materials having some mesoporous character through the addition of a co-template. In the present paper, we chose surfactant tetrapropyl-ammonium bromide as a template and systematically investigated the effects of the presence of various molar ratios of xylitol ions (Xy) on the nature of the products obtained. The role of the co-template Xy in the synthesis of microporous materials was also discussed in addition to clarifying the role of adding Xylitol on the crystallinity, crystals size and thermal stability of ZSM-5 zeolites produced. The synthesized ZSM-5 materials were examined by N_2 adsorption, XRD, FTIR, TG/DSC and Pyridine adsorption.

Experimental

Reagents used in zeolite synthesis

The silica source employed was silicic acid powder (prepared in this work).

Alkaline source was Sodium hydroxide pellets (A.R 98%).

The Alumina source employed was Aluminum Sulfate [Merck, $Al_2(SO_4)_3 \cdot 16H_2O$; 99%].

Template sources employed for all synthesis were purchased from Aldrich and they are: Teterapropy-lammonium bromide (TPA-Br; 99.5%) and Xylitol (Xy; 99%). The used commercial acids were H_2SO_4 and HCl.

Preparation of silicic acid

The silicic acid was prepared by precipitation from commercial sodium silicate with 20% HCl. The precipitate was washed several times with water to remove chloride ions that were checked regularly by using a solution of $AgNO_3$ (0.1 M). The precipitate was dried at 120 °C for 4 h in an air oven.

Effect of template

The batch preparations composed of molar ratios of following formula were as:

1.04 Na_2O:0.13 Al_2O_3:8.5 SiO_2:33.2 TPA-Br:6.32 NPA:300 H_2O
1.04 Na_2O:0.13 Al_2O_3:8.5 SiO_2:16.6 TPA-Br:n-Xylitol:300 H_2O
1.04 Na_2O:0.13 Al_2O_3:8.5 SiO_2:16.6 TPA-Br:300 H_2O
1.58 Na_2O:0.13 Al_2O_3:10.5 SiO_2:m-Xylitol:300 H_2O

Where n = (4.0, 5.3, 6.7, 9.6, 14, 33 and 50) gm dl^{-1} and m = (40, 50, 58 and 67) gm dl^{-1}. Silicic acid, aluminum sulfate and sulfuric acid were used during these batch preparations. The crystallization temperature was fixed between 120 and 160 °C while the crystallization period was varied between 2 and 6 days.

Zeolite synthesis

A specific amount of NaOH was added to silicic acid in a small amount of H_2O (40 ml) while stirring, followed by heating at 80 °C until a clear solution was reached. The template (any one of them or mixture of both; TPA-Br + Xy) was dissolved in a little amount of H_2O (20 ml) with heating at 50 °C for 20 min. The solution of template was added to that of sodium silicate solution whilst stirring for 15 min. The aluminum

sulfate, on the other hand, was dissolved in a small amount of H_2O (10 ml) while adding 0.05-ml concentrated H_2SO_4 with stirring until reaching a clear solution. To the latter solution, the combined solution of sodium silicate and the template was added followed by stirring for 30-min. The pH of the mixture was adjusted at 11 by using NaOH (0.1 M) and H_2SO_4 (0.1 M) solutions. Finally, the mixture was hydrothermally treated at 160 °C in an oil bath, using stainless steel autoclaves, for 2–6 days. The autoclaves were removed at the specified time from the oil bath and quenched immediately with cold water. The solid product was filtered and washed with distilled water until the pH of the filtrate dropped to 8. The products were dried at 110 °C for 10 h then calcined at 550 °C for 6 h in an air oven.

Experimental techniques

The X-ray diffractograms of various zeolitic samples were measured by using a Philips diffractometer (type PW 3710). The patterns were run with Ni-filtered copper radiation ($\lambda = 1.5404$ Å) at 30 kV and 10 mA with a scanning speed of $2\theta = 2.5°$ min^{-1}. The crystal sizes of the prepared materials were determined using the Scherrer equation. The instrumental line broadening was measured using a LaB$_6$ standard. The crystallinity of the prepared samples was calculated using the ratio of the sum of the areas of the most intense peaks for ZSM-5 samples ($2\theta = 20–25°$) to that of the same peaks for the standard (Na-ZSM-5 Mobil chemicals) and multiplying by 100. The difficulty of evaluating the crystallites size by XRD technique have been overcome by the help of new methods of the structural refinement; the Rietveld one, that permits the reproduction of the whole diagram, through the optimization of both structural (peak position and intensity) and non-structural (peak shape) data. This indeed, facilitates measuring the crystallite size in a more accurate way.

FT-IR spectra of the samples were recorded with a JASCO single beam FT-IR 5300-spectrometer with 50 co-added scans at 2 cm^{-1} resolution. All IR measurements were carried out at room temperature using KBr technique.

Thermogravimetric and differential scanning calorimetry (TG/DSC) were carried out using Shimadzu-50 thermal analyzer units. The sensitivity of TG and DSC measurements was 0.01 mg and 25 μv, respectively. In each run about 10 mg of uncalcined sample was heated from room temperature to 1,000 °C at a heating rate of 10 °C min^{-1} in a current of N_2 flowing at a rate of 30 ml min^{-1}.

The nitrogen adsorption isotherms were measured at –196 °C using a conventional volumetric apparatus. The specific surface area was obtained using the BET method. Samples were out-gassed at 300 °C for 3 h at a reduced pressure of 10^{-5} Torr prior to admitting N_2 gas. The micropore volume and the external surface area were obtained from the t-plot method.

Thin, but intact, self-supporting wafers (30 ± 5 mg cm^{-2}) of the adsorbents were prepared and mounted inside a specially designed, heatable and evacuable, all quartz glass IR cell. The cell containing samples, equipped with CaF$_2$ windows, was hooked to a pyrex glass Gas/Vac handling system and evacuated to 10^{-5} Torr at 300 °C prior subjecting to 10 Torr portion of pyridine vapor that was expanded at 25 °C at which adsorption of Py takes place. A spectrum of the gas phase was recorded before a 5 min degassing of the cell (at 25 °C) and taking a spectrum of the wafer plus irreversibly adsorbed pyridine. By absorption subtraction of the cell and wafer, IR difference spectra of the gas phase and Py adsorbed species were obtained, respectively.

Results and discussion

Surface texturing

The different surface characteristics of various synthesized ZSM-5 zeolites as a function of varying templates were determined from nitrogen adsorption–desorption isotherms conducted at –196°C. These characteristics include BET surface area (S_{BET}), total pore volume (V_P^t) micro- and wide pore volume (V_P^u, V_p^W), micro- and wide surface area (S^u, S^w), external surface area (S^{ext}) and mean pore radius (r). The obtained isotherms (Fig. 1) are closely belong to the mixed type I and II of Brunauer classification [17]. At high p/p^o, some deviation from type I isotherm was observed along with desorption hystersis for the sample produced from TPA-Br + Xy. This may be due to intra-crystalline mesopores that have been validated from V_I–t plots (Fig. 2). The specific surface areas of investigated ZSM-5 zeolites that were determined from the linear BET plots, were found to be in the following orders (see Table 1):

$$TPA\text{-}Br > TPA\text{-}Br + Xy > Xy$$

The total pore volume follows the same order as that of the specific surface area. Such congruent changes in area and pore volume resulted in the following order of r:
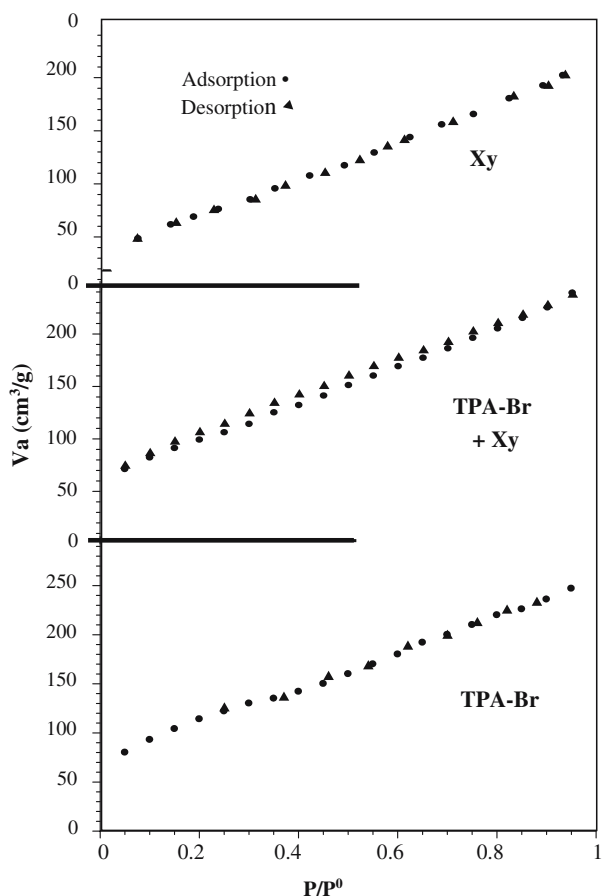
Fig. 1 Nitrogen adsorption–desorption isotherms of ZSM-5 Zeolites synthesized by using different templates. Conditions of the preparation. SiO_2/Al_2O_3 molar ratio 64 except sample (Xy) 81, Na_2O/SiO_2 molar ratio 0.121 except sample (Xy) 0.228, hydrothermal time 2 days except sample (Xy) 6 days, hydrothermal temperature 160 °C, Xylitol 9.6 gm dl^{-1} except (Xy) 67 TPA-Br 16.6 gm dl^{-1}

Fig. 2 V_1–t plots of Na ZSM-5 materials synthesized using various templates

$$Xy > Xy + TPA\text{-}Br \approx TPA\text{-}Br$$

This indicates that the noted increase in r for ZSM-5 derived from the template Xy affected greatly the surface area of this sample to be the lowest between all samples. This decrease in surface area was about 27% of the specific surface area exerted by ZSM-5 derived from the template TPA-Br. This marked decrease could be due to the irregular decrease in crystallinity of ZSM-5 produced when using Xy as a template, as will be elaborated later by XRD investigations. The specific areas calculated from V_1–t plot were found to be in a good agreement with those evaluated from BET. This verifies the correct choice of the reference t values of Lecloux and Pirard [18] that depends on the BET-C constant values. The V_1–t plots of ZSM-5 derived from Xy and Xy + TPA-Br templates; depicted in Fig. 2,
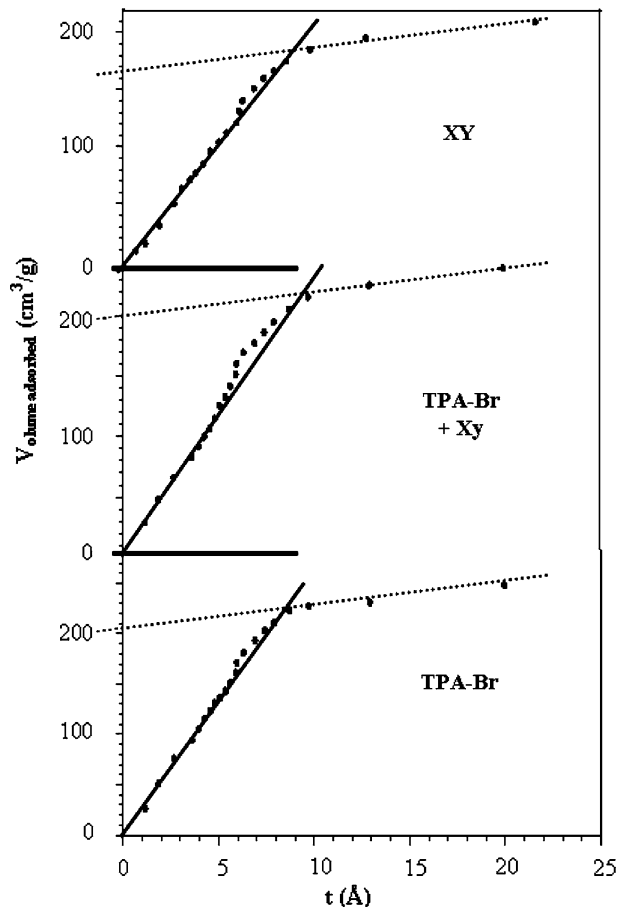
showed a small upward deviation bounded by downward deviations at low and high t values, indicating the heterogeneity of the texture thus, being narrow and wide pores. The V_1–t plot of ZSM-5 derived from TPA-Br + Xy template shows that some points in the t range 5.2–8.8 Å lie just over the straight line extended to pass through the origin before the start of the downword deviation at t = 9.0 Å. The size of the upward deviation indicates the existence of a number of pores of sizes in the lower limit of mesopores. A more detailed information of N_2 adsorption–desorption isotherms is summarized in Table 1. The micropore volume of the samples is in the range 0.26–0.38 cm^3 g^{-1} [19], which is higher than that of pure silicalite nanocrystals (ca. 0.19–0.20 cm^3 g^{-1}), and ZSM-5 (0.140 cm^3 g^{-1}) [20], indicating the high crystallinity of our prepared samples comparatively. The external surface area S_{ext} of ZSM-5 derived from TPA-Br + Xy (36.3 m^2 g^{-1}), calculated from the slope of the V_1–t curve was higher than that derived from either Xy (31.6) or TPA-Br (31.75) confirming that latter samples preserve higher microporous texturing. This microporosity was also

Table 1 Some surface characterization of different templates investigation adsorbents, heated at 300 °C under a reduced pressure of 10^{-5} torr

Templates	S_{BET}	S_t	V_p^t	r (Å)	C_{const}	S^u	S^{ext}	V_p^u	V_p^{wid}	S^{wid}	Microporosity (%)
Xy	303	308	0.315	25.9	20	252	31.6	0.262	0.053	55	83
TPA-Br + Xy	393	386	0.369	23.4	46	322	36.29	0.302	0.067	64	81
TPA-Br	415	424	0.382	23.0	83	352	31.75	0.324	0.058	72	84

S_{BET}, BET surface area $m^2\ gm^{-1}$; S_t, surface area derived from V_1–t plot $m^2\ gm^{-1}$; S^{wid}, wide pore surface area $m^2\ gm^{-1}$; S^u, microporous surface $m^2\ gm^{-1}$; V_p^{wid}, the volume adsorbed in wide porous ($cm^3\ gm^{-1}$); V_p^u, micropore volume ($cm^3\ gm^{-1}$); r (Å), average pore radius; V_p, the total pore volume at $p/p^o = 0.95$ ($cm^3\ gm^{-1}$); S_{ext}, external surface area of micropores ($m^2\ gm^{-1}$); microporosity (%) = $V_p^u/V_p^t \times 100$

emphasized by the percentage microporosity ($V_p^u/V_p \times 100$) that attained 83–84% for ZSM-5 samples synthesized using Xy and TPA-Br. Thus, one can attribute the decrease in S_{BET} of the sample derived from Xy when compared with TPA-Br to the decreased crystallinity of the former comparatively. Of particular importance, NPA has been used as an initiator during synthesizing ZSM-5 utilizing TPA-Br since it helps in nucleation and crystallization processes. Amines affect the zeolite structure through the amine molecule shape and their effects were secondary to the effect of Al concentration in the reaction mixture [21]. This point is worthy for a further study.

Morphological analysis of ZSM-5 as traced by XRD

ZSM-5 samples with different degrees of crystallinity and crystals size, which obtained when using different templates were shown in Fig. 3. Experiments with initial silica/alumina ratio 64 after 48 h of crystallization at 160 °C produced ZSM-5 in case of using TPA-Br and TPA-Br + Xy those permit, respectively, values of crystallinity comparable and higher than 100% when compared with ZSM-5 purchased from Mobil of same silica/alumina ratio. ZSM-5 prepared with Xy template exhibits a decrease in crystallinity comparatively and shows an additional high intense peak of silica phase ascribed to SiO_2-quartz [22]. The XRD characterization data of the produced ZSM-5 as a function of using different templates including cell constant, cell volume, percentage crystallinities and particles size are presented in Table 2. These data were also refined using full prof-98 program that showed a good agreement between calculated and observed patterns. The relative XRD crystallinity (crystallinity %) calculated with respect to the standard sample that taken at 100% crystallinity and possessed the same SiO_2/Al_2O_3 molar ratio, was based on summation of the peaks height at 2θ equal 23.4, 24 and 24.4. The above results indicate that mixing of TPA-Br surfactant with some other template might induce some effects during the crystallization process. Interestingly, using a template other

than tetralkylammonium ions or molecules (e.g. amines) for directing the pentasil ZSM-5 framework structure was obtained when using Xy that exhibited crystallinity comprises of 71%. Although ZSM-5 produced from Xy seems to have low XRD crystallinity, it showed the highest yield (65%) at the end of the synthesis process as well as small crystallites size. The synthesis of such ZSM-5 with small crystallites size points to a high rate of nucleation when using Xy as template. The existence of a separate phase of silica might be responsible for decreasing the crystallites size due to decreasing the silica/alumina ratio thus exposing excess aluminium so as to initiating the formation of small crystals [23]. The increase in the degree of crystallinity in the produced ZSM-5 as a function of adding Xy to TPA-Br could be due to the role of hydrogen bonding of O···H+ groups in Xy in increasing the rate of nucleation of ZSM-5 phase. This increase

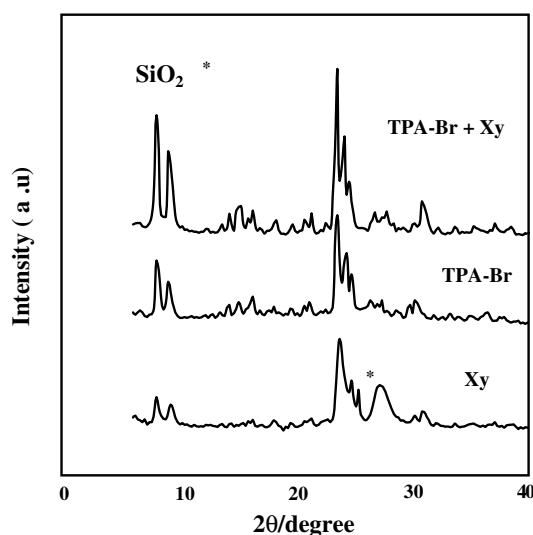**Fig. 3** X-ray diffraction patterns of ZSM-5 zeolite synthesized using different templates. Conditions of the preparation: SiO_2/Al_2O_3 molar ratio 64 except sample (Xy) 81 molar ratio, Na_2O/SiO_2 molar ratio 0.121 except sample (Xy) 0.228 molar ratio, hydrothermal time 2 days, hydrothermal temperature 160 °C, TPA-Br 16.6 gm dl^{-1}, Xy 9.6 gm dl^{-1} except (Xy) 67

Table 2 The XRD characterization data of the produced ZSM-5 zeolite as a function of using different templates

Templates	Cell parameters (Å)			V (Å^3)	Cryst. %	B /rad	Particle size (nm)
	a	b	c				
Xy	19.556	20.105	13.357	5,251.6	71	0.00319	40.5
TPA-Br	19.440	20.094	13.356	5,251.9	100	0.00349	61
TPA-Br + Xy	19.562	20.084	13.353	5,246.1	142	0.00349	61
ZSM-5 (Reference)	20.00	19.690	13.380	5,269.0			

may lead to an effective decrease in the time necessary for crystal growth of ZSM-5 phase to be two days upon addition of Xy. Such effect can also be explained by a possible increase in the dissolution of the gel phase by increasing the polyalcohol Xy groups. Increasing the molar ratio of Xy from 9.6 when using mixed template to 67 in synthesizing ZSM-5 by the sole template Xy is most likely due to the decreased partial positive charge present on intramolecular hydrogen bonding of OH groups; in Xy, that can hardly satisfy the negative charge positioned on Al–O$^-$ moieties.

The mixed templates of TPA-Br and Xy affect the change of the packing parameter, and ordered microporous structures, in such way to produce the favored ZSM-5 pentasil structure. Similar results were observed in the mesoporous silica [24–26]. Huo et al. [27, 28] proposed a generalized mechanism of formation based on the specific type of electrostatic interaction between a given inorganic precursor I and surfactant head group S. By extension, another charge-interaction pathway was S$^+$X$^-$I$^+$, where S$^+$ was the structure director, I$^+$ was the inorganic precursor, and X was a counterion. Accordingly cationic oxide species primarily composed of silica (I$^+$) plus the surfactant templating agent TPA$^+$(S$^+$) could be used to synthesize micro-mesostructured ZSM-5. The X (halide anions such as Br$^-$ and OH$^-$) became involved through this pathway, as it served to buffer the repulsion between S$^+$ and I$^+$ by means of weak hydrogen-bonding forces. The interactions between the surfactant molecules (TPA$^+$) and the inorganic counterions (AlO$^-$, OH$^-$) can postpone the combination of the inorganic ions, and the self-assembly of inorganic materials and surfactant molecules will prefer to take place in such a way as to form a micro-mesophase through hydrogen bonding interactions. According to this mechanism, OH should self-assemble around the cationic surfactant (TPA-Br) molecules before the addition of both silica and alumina solutions, so that the latter ions can be attracted by the gathered OH$^-$ to form ZSM-5 structure.

From what has been presented so far, it has been shown that ZSM-5 synthesized by Xy + TPA-Br indicated superior crystallinity when compared with others

as well as micro-mesopores surface, which can used in surface driven applications. Thus a more attention was paid to this system in comparison with the individual analog derived from TPA-Br through varying the ratios of Xy/TPA-Br aimed at explaining the present morphological and surface properties.

Thermal analysis

Figure 4 shows TG and DSC curves of uncalcined ZSM-5 synthesized using TPA-Br template while being heated in N$_2$ atmosphere. It is obvious that the weight loss occurs in three steps: the first between 25 and 400 °C due to desorption of water and comprises a weight loss of 0.8%, the second step, between 420 and 500 °C, due to thermal decomposition of TPA$^+$ ions occluded in various types of pores and comprises a weight loss of 8% and the third, between 500 and 850 °C that comprises 0.3% weight loss and ascribed to elimination of H$_2$O during condensation of surface hydroxyl groups and/or removal of chemically bound water. DSC, on the other hand, shows four endothermic peaks at 100, 470, 591 and 875 °C. As it can be seen, the third weight loss occurred in the 500–850 °C range (TG curve) consists of two endothermic peaks positioned at 591 and 875 °C. Accordingly, ascribing
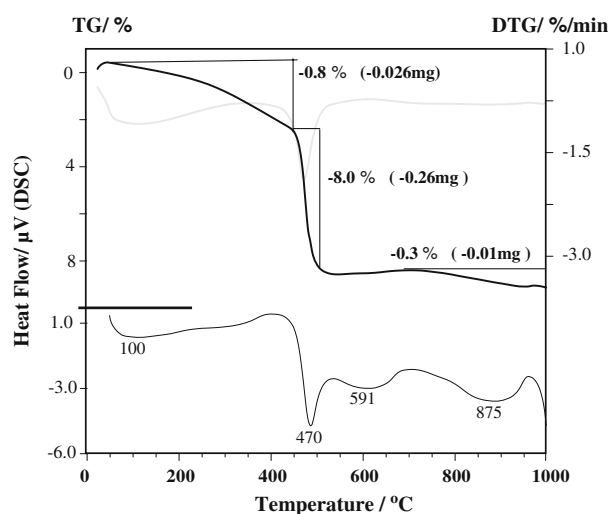
Fig. 4 TG/DSC curves for ZSM-5 zeolite prepared by TPA-Br

the 591 °C peak to elimination of H_2O during condensation of surface OH group is unlikely but indeed could be due to thermal decomposition of TPA^+ molecules occluded in narrow pores. This is confirmed from lowering the total mass loss of TPA^+ (8.0%) than that of the calculated value (11.7%), assuming four TPA^+ cations per unit cell in a pure ZSM-5 crystal. One can also notice that the thermal stability of ZSM-5 prepared by TPA-Br is remained till heating to 1,000 °C.

Figure 5 shows TG and DSC curves obtained for uncalcined ZSM-5 synthesized using the TPA-Br + Xy (obtained at 160 °C) template while being heated in N_2 gas. It is obvious that this sample is stable to heating up to 380 °C. Following the latter temperature the sample is shown to commence losing mass with a fast and sharp step till 500 °C involving a total mass loss comprises of 8%. The following step started from 500 to 1,000 °C and did not indicate a mass loss and rather showed a horizontal line reflecting the high thermal stability of the sample. The behavior of decomposition steps during ramping the temperature is different suggesting some effects due to Xy involvement although the total weight loss of this sample (8.1%) is almost similar to that synthesized by TPA-Br. The DSC curve of ZSM-5 synthesized using TPA-Br + Xy shows varying effects when compared with that resulted from TPA-Br. The former indicates an exothermic peak at 420 °C recognized to carbonaceous oxidation products as a result of Xy decomposition together with an endothermic peak at 470 °C similar to the one seen in ZSM-5 derived from TPA-Br. Unexpectedly, addition of Xy into TPA-Br affected the multistep decomposition seen in DSC thermogram of the sample derived from TPA-Br especially those at 591 and 875 °C giving a broad endothermic peak in the
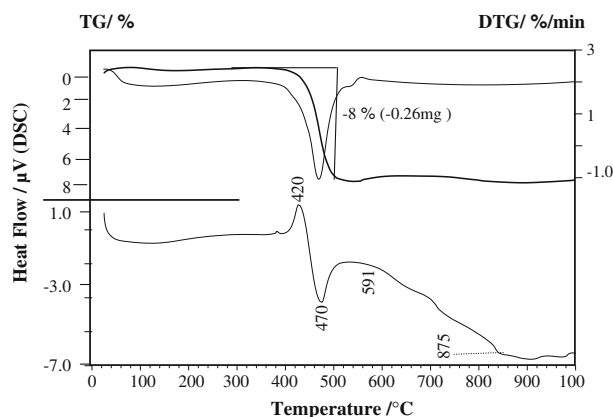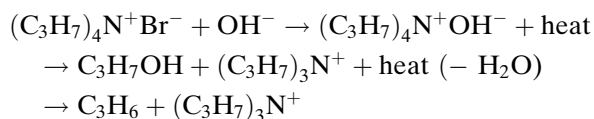
range from 500 to 1,000 °C point to decreasing the pore radius of the sample derived from TPA-Br + Xy when compared with TPA-Br and thus indicates appreciable microporosities together with mesoporosities. The weight loss in ZSM-5 derived from TPA-Br + Xy (8.1%) is significantly less than that required to form a well-defined unit cell (18.4%), assuming four TPA^+ + Xy cations per unit cell in a pure ZSM-5 crystal. This could indicate the presence of appreciable amounts of TPA^+ + Xy molecules enclosed inside the pores of ZSM-5 Zeolite. In addition, this particular sample showed a higher hydrophobic tendency comparatively and hence higher accessibility to many potential molecules based on neglecting the selectivity during adsorption processes occurring before any catalytic events.

From the foregoing studies [2, 4, 8, 9] concerning decomposition of TPA-Br, it can be concluded that a decomposition step into alcoholic product (mostly propanol) is expected together with $(C_3H_7)_3N^+$ moieties that underwent to further decompositions, as can shown in the following scheme.

$$(C_3H_7)_4N^+Br^- + OH^- \rightarrow (C_3H_7)_4N^+OH^- + heat$$
$$\rightarrow C_3H_7OH + (C_3H_7)_3N^+ + heat \ (- H_2O)$$
$$\rightarrow C_3H_6 + (C_3H_7)_3N^+$$

Hence, addition of xylitol (polyol) might constitute with C_3H_7OH a common ion effect hence a reverse reaction can be expected to maintain $(C_3H_7)_4N^+OH^-$ for longer time working in organizing different substrates into pentasil ZSM-5 structure. Thus, an expected formation of $(C_3H_7)_4 N^+ O^- \cdots H^+ \cdots O^- R$ linkages can be estimated as an influence of mixing templates explaining the highest crystallinity obtained between all studied templates.

Fourier transform Infrared study of ZSM-5 produced as a function of various templates

The infrared spectra of the lattice modes obtained for the various ZSM-5 samples produced by using different templates are shown in Fig. 6. It can be seen that, the wavenumber of external asymmetric stretching mode at 1,090 cm^{-1} [24], showed a shift to higher wavenumber upon varying the templates, e.g. at 1,097 cm^{-1} in Xy + TPA-Br and at 1,099 cm^{-1} in TPA-Br. Similarly, v_{as} (T–O) at 1,224 cm^{-1} showed a shift into 1,230 cm^{-1} in Xy + TPA-Br demonstrating the strength of these modes when adding Xy into TPA-Br. This could give a clue on the effect of various templates in structuring the framework bonds in ZSM-5 Zeolite. These spectra
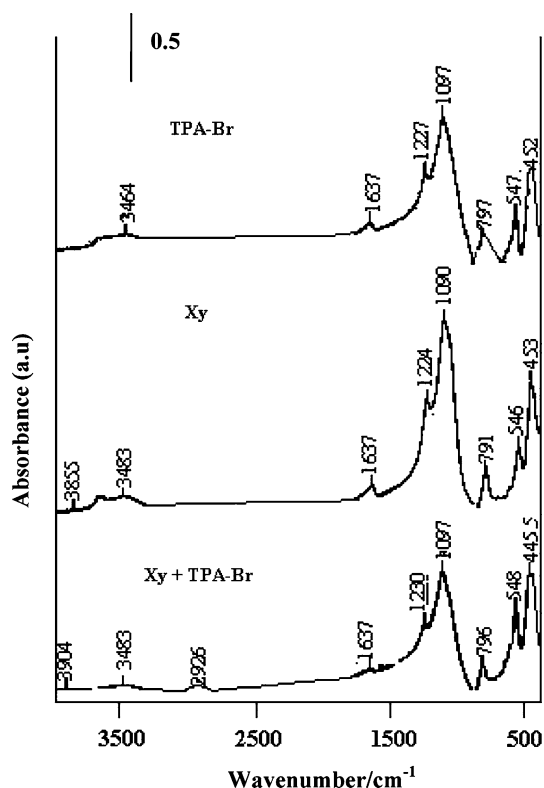
Fig. 5 TG/DSC curves for ZSM-5 zeolite prepared by TPA-Br + Xy

those appearing at 3,750 cm⁻¹. These bands are, respectively, due to acidic OH groups, extra framework Al species and free silanol groups. Interestingly, the deformation band of water positioned at 1,637 cm⁻¹ is almost vanished in the zeolite sample resulted from Xy + TPA-Br reflecting the hydrophobicity of this material, comparatively.

Acidity evaluation

The FTIR spectra of adsorbed Pyridine (Py) given in Fig. 7 have been collected at 25 °C for ZSM-5 samples synthesized using different templates, in order to investigate the nature as well as to estimate the number of acidic sites of ZSM-5 produced. This figure compares νccN spectra of Py adsorbed on ZSM-5 samples synthesized using Xy, TPA-Br and TPA-Br + Xy templates. The spectra of Py/ZSM-5 that derived from using TPA-Br template displays bands indicative of hydrogen bonded Pyridine; HPy (at 1,438 cm⁻¹), Lewis Pyridine; LPy (1,458, 1,490, 1,636 cm⁻¹) and Brönsted Pyridine; BPy (at 1,541, 1,648 and 1,653 cm⁻¹) species. In addition, a band at 1,560 cm⁻¹ is observed and could be correlated to either HPy or to $\delta N^+–H$ vibrations [29]. It is worth mentioning that this band cannot be ascribed to α-Pyridone species ($\nu C=O$), i.e. excluding the existence of basic Al–O⁻ groups in the Zeolite structure. In view of the above results, chemisorption of Py on ZSM-5 at 300 K is shown to lead to formation of LPy species bounded essentially to cus Al³⁺ species through 1,636 and 1,458 cm⁻¹ bands whose depicted at higher wavenumbers than those assembled by octahedral ones (1,614 and 1,450 cm⁻¹) [30]. This indicates the involvement of alumina with silica in a fairly fit tetrahedral array constituting the ZSM-5 framework. The occurrence of the 8a mode of vibration at two different frequencies (1,648 and 1,654 cm⁻¹) may account for the involvement of two different types of Brönsted acid sites. The data complied in Table 4 gives an idea about the position and concentration of Brönsted and Lewis acid sites and their ratios BPy/LPy under equilibrium condition of Py adsorption at 300 K. The correlation resulting from our experimental data, and presented in Table 4, that allowed the determination of CL and CB

Fig. 6 FTIR absorbance spectra of ZSM-5 zeolites prepared by using different templates

exhibit in addition typical vibrations of ZSM-5 positioned at 452(445), 545(546) and 791(797) cm⁻¹. The band at 546–548 cm⁻¹ had been assigned by Jacobs et al. [25] to highly distorted double five membered rings present in the ZSM-5 structure. The absorbance at this frequency has been utilized [25] to estimate the IR crystallinity of the materials in relative to that at 452 cm⁻¹. The latter phenomenon was calculated and presented in Table 3 together with the framework vibrational frequencies. No vibration modes were detected for external linkage of five membered ring (590–620 cm⁻¹), [26] revealing the effect of template in determining the stretching vibration of MFI produced.

A broad band in the hydroxyl region between 3,700 and 3,000 cm⁻¹ with a maximum at ca. 3,483 cm⁻¹ was depicted in ZSM-5 derived from Xy and Xy + TPA-Br where at 3,464 cm⁻¹ in TPA-Br. Bands appearing at 3,650 cm⁻¹ and 3,674–3,680 cm⁻¹ were shown besides

Table 3 Mid-IR frequencies (cm⁻¹) of tetrahedral vibrations of T(Si or Al)–O and crystallinities (peak area of 545/450) of NaZSM-5 as a function of employed templates

Template	ν_{as} (T–O) 850–1,350 cm⁻¹	ν_{s} (T–O) 620–850 cm⁻¹	ν (T–O) stretching mode	ν (T–O) deformation mode	545/450
Xy + TPA-Br	1,230, 1,097	796	548	445	0.7
Xylitol	1,224, 1,090	791	546	453	0.21
TPA-Br	1,227, 1,097	797	547	452	0.46

Fig. 7 FT-IR absorbance spectra of pyridine adsorbed on ZSM-5 zeolite prepared by different templates

framework [31]. The presence of the alkali cation enhances the electron density of the framework oxygen and thus can act as basic sites. The strength of these sites depends on the structure of the framework, chemical composition and on the nature of the counter cation [32, 33]. Accordingly, one can expect that an excess of the TPA-Br template plays the same role as the alkali metal cation do in provoking and stabilizing the basic sites. Indeed, there is less information on basic sites in zeolite and also in zeolites possess both Brönsted and basic sites [34]. Stimulation of these sites can result in a big area in catalytic application of zeolites but also could lead to loss of selectivity in some reactions [35]. The acidity of the ZSM-5 sample derived from using Xy + TPA-Br template was in the middle between the other two samples and showed an increase in Brönsted acid sites comparatively. Of particular interest, the conversion of LPy into α-Pyridone on alumina surfaces has been taken place at higher temperature as high as 327 °C [36]. However, revealing such species on ZSM-5 at 25 °C implies the presence of Al–OH$^-$ groups, that could attack α-carbons of co-ordinated Py and thus forming α-Pyridone. Increasing the density of Brönsted acid sites in our synthesized ZSM-5 samples is obviously related to the framework Al content.

Conclusions

ZSM-5 produced when using Xylitol as a new template showed the highest yield (65%), maximum pore radius (26 Å) and smallest crystallites size (41 nm) between all samples. However, this zeolite sample presented also the lowest degree of crystallinity (71%), lowest S_{BET} (303 m^2 g^{-1}) and lowest acidity. In a way of optimizing the texture properties, thermal stability, crystallinity, and acidity of ZSM-5 produced, addition of Xylitol to TPA-Br was accomplished and revealed the following outcomes:

1. Increasing the crystallinity percentages (140%), and the size of the crystals (61 nm).
2. Enhancing both the thermal stability and hydrophobicity character of the produced ZSM-5 zeolite.

were evaluated based on the molar absorptivities of ε_L (0.64 ± 0.4) cm μmol^{-1} and ε_B (0.73 ± 0.04) cm^{-1} μmol^{-1}, respectively. Thus, the over all amount of chemisorbed Pyridine can be evaluated. Similarly, the above-mentioned bands are also observed on ZSM-5 samples derived from using either Xy or Xy + TPA-Br templates but at lower intensities. The 1,456 cm^{-1} band seems to improve slightly in ZSM-5 derived from using Xy, reflecting a decrease in the B/L ratio (Table 4). The prominent presence of the 1,558–1,560 cm^{-1} band even after evacuation at 473 K (not shown) excludes the previous assignment ascribing it to HPy and indeed strengthens its attribution to δN$^+$–H vibration (BPy). Accordingly, the restoration of the band following outgassing at 473 K also remind us by α-Pyridone species. The existence of basic sites in zeolites could be correlated directly with the alkali Na$^+$ cations, which compensate the negative charge cited on the

Table 4 The effect of template on the position and concentration of Lewis and Brönsted acid sites of synthesized NaZSM-5 zeolites

Name	LPY (υcm^{-1})	BPY (υcm^{-1})	C.L L.Py μmol cm^{-2}	C.B L.Py μmol cm^{-2}	nPy = nB + nL	C.B/C.L
TPA-Br	1,458	1,541	2.56	5.84	8.4	2.28
Xylitol + TPA-Br	1,457	1,540	2.68	3.06	5.74	1.14
Xylitol	1,456	1,539	3.28	2.19	5.47	0.66

3. Enhancing the surface area of the produced ZSM-5 that renders as well a mesoporous texture.

4. Formation of reactive basic sites besides those of acidic ones (composed mainly of Brönsted acidity) proposing the presence of acid–base pair sites.

References

1. Tanabe K, Misono M, Ono Y, Hattori H (1989) In: Delmon B, Yates JT (eds) New solid acids and bases, their catalytic properties, studies in surface science and catalysis, vol 51. Elsevier, Amsterdam
2. Salama TM, Mohamed MM, Othman I, El-Shobaky GA (2005) Appl Catal A 286:85
3. Csicsery SM (1976) In: Rabo JA (ed) Zeolite chemistry and catalysis, chapter 12, ACS Monograph, vol 171. American Chemical Society, Washington
4. Mohamed MM, Othman I, Eissa NA (2005) Micropor Mesopor Mater 87:93
5. Mohamed MM, Eissa NA (2003) Mater Res Bull 38:1993; Ramamurthy V (2000) J Photochem Photobiol C 1:145
6. Richter M, Berndt H, Eckelt R, Schneider M, Fricke R (1999) Catal Today 54:531; Matsuoka M, Anpo M (2003) J Photochem Photobiol C 3:225
7. Beck JS, Vartuli C, Roth WJ, Leonowicz ME, Kresge CT, Schmitt KD, Chu CT-W, Olson DH, Sheppard EW, McCullen SB, Higgins JB, Schlenker JL (1992) J Am Chem Soc 114:10834
8. Beck JS, Vartuli JC, Kennedy GJ, Kresge CT, Roth WJ, Schramm SE (1994) Chem Mater 6:1816
9. Bergstrom M (2001) Langmuir 17:993
10. Patist A, Devi S, Shah DO (1999) Langmuir 15:7403
11. Khan A, Marques EF (1999) Curr Opin Colloid Int 4:402
12. Zana R, Michels B (1998) Langmuir 14:6599
13. Aramaki K, Kunieda H (1999) Colloid Polym Sci 277:34
14. Shiloach A, Blankschtein D (1998) Langmuir 14:7166
15. Shiloach A, Blankschtein D (1998) Langmuir 14:1618
16. Huang L, Chen X, Li Q (2001) J Mater Chem 11:610
17. Brunauer S, Deming LS, Deming WE, Teller EJ (1940) Am Chem Soc 62:1723
18. Lecloux A, Pirard JP (1979) J Colloid Interface Sci 70:265
19. Olson DH, Haag WO, Lago RM (1980) J Catal 61:390
20. Gervasini A (1999) Appl Catal 180:7
21. Vedrine JC (1992) In: Derouane EG (ed) Zeolite microporous solids: synthesis, structure and reactivity. Kluwer Academic, The Netherland, p 107
22. Van Geem PC, Scholle KF, Van der Velden GPM, Veeman WS (1988) J Phys Chem 91:158
23. Hincapie BO, Garces LJ, Zhang Q, Sacco A, Suib SL (2004) Micro Meso Mater 67:19
24. Jacobs PA, Bayer HK, Valyon J (1981) Zeolites 1:161
25. Jacobs PA, Derouane EG, Weit KG (1981) J Chem Soc Chem Commun 12:591
26. Kulkarne SB, Shirakar VP, Kotasthan AN, Borade R, Ratnasamy BP (1982) Zeolite 2:313
27. Huo QS, Margolese DI, Ciesla U, Feng P, Gier TE, Sieger P, Leon R, Petroff PM, Schuth F, Stucky GD (1994) Nature 368:317
28. Huo QS, Margolese DI, Ciesla U, Feng P, Gier TE, Sieger P, Firouzi A, Chmelka BF, Schuth F, Stucky GD (1994) Chem Mater 6:1176
29. Boccuti MR, Rao KM, Zecchina A, Leofanli G, Pertrini Y (1989) In: Morlerra L, Zecchina A (eds) Structure and reactivity of surfaces. Amsterdam, p 133
30. Urban MW (1993) Vibration spectroscopy of molecules and macromolecules on Surfaces. Wilery, Chichester, pp 171–185
31. Pophal C, Yogo T, Tamada K, Segawa K (1998) Appl Catal B 16:177
32. Knozinger H (1976) Adv Catal 25:184
33. Martra G, Ocule R, Marchese L, Centi G, Coluccia S (2002) Catal Today 73:83
34. Barthomeuf D (1996) Cat Rev Sci Eng 38:521
35. Barthomeuf D, Mirodatos C, Vedrine JC (1988) J Phy Chem 92:1637
36. Zaki MI, Hassan MA, Al-Sagheer FA, Pasuplety L (2001) Colloid Surf A 190:261